Understanding the O-17 excess glacial-interglacial variations in Vostok precipitation

Camille Risi, Amaëlle Landais, Sandrine Bony, Jean Jouzel, Valérie Masson-Delmotte, Francoise Vimeux

JOURNAL OF GEOPHYSICAL RESEARCH, VOL. 115, D10112, doi:10.1029/2008JD011535, 2010

Understanding the ^{17}O excess glacial-interglacial variations in Vostok precipitation

Camille Risi,[1] Amaelle Landais,[2] Sandrine Bony,[1] Jean Jouzel,[2]
Valérie Masson-Delmotte,[2] and Françoise Vimeux[3]

Received 27 November 2008; revised 30 October 2009; accepted 16 December 2009; published 29 May 2010.

[1] Combined measurements of $\delta^{18}O$, $\delta^{17}O$, and δD in ice cores, leading to d excess and ^{17}O excess, are expected to provide new constraints on the water cycle and past climates. We explore different processes, both in the source regions and during the poleward transport, that could explain the ^{17}O excess increase by 20 per meg observed from the Last Glacial Maximum (LGM) to Early Holocene (EH) at the Vostok station. Using a single-column model over tropical and subtropical oceans, we show that the relative humidity at the surface is the main factor controlling ^{17}O excess in source regions. Then, using a Rayleigh-type model, we show that the ^{17}O excess signal from the source region is preserved in the polar snowfall, contrary to d excess. Evaporative recharge over mid and high latitudes and $\delta^{18}O$ seasonality in polar regions can also affect the Vostok ^{17}O excess but cannot account for most of the 20 per meg deglacial increase from LGM to EH. On the other hand, a decrease of the relative humidity at the surface (rh_s) by 8 to 22% would explain the observed change in ^{17}O excess. Such a change would not necessarily be incompatible with a nearly unchanged boundary layer relative humidity, if the surface thermodynamic disequilibrium decreased by 4°C. Such a change in rh_s would affect source and polar temperatures reconstructions from $\delta^{18}O$ and d excess measurements, strengthening the interest of ^{17}O excess measurements to better constrain such changes.

Citation: Risi, C., A. Landais, S. Bony, J. Jouzel, V. Masson-Delmotte, and F. Vimeux (2010), Understanding the ^{17}O excess glacial-interglacial variations in Vostok precipitation, *J. Geophys. Res.*, *115*, D10112, doi:10.1029/2008JD011535.

1. Introduction

[2] Stable isotopic measurements of water ($\delta^{18}O$ and δD) have been performed for more than 50 years [*Dansgaard*, 1953; *Epstein and Mayeda*, 1953; *Craig*, 1961] with the aim to improve our understanding of the water cycle and its links to climate. At first order, variations of $\delta^{18}O$ and δD are mainly due to the difference in saturation vapor pressures between the light and heavy isotopes, leading to an equilibrium fractionation. In addition, the larger diffusivity of light isotopes with respect to the heavy ones results in a kinetic fractionation, involved in evaporation and in snowflakes formation. Since these kinetic effects have a larger influence on $\delta^{18}O$ than on δD [*Merlivat and Nief*, 1967; *Merlivat*, 1978], there is an added value in combining $\delta^{18}O$ and δD measurements.

[3] This second-order effect is measured by d excess = $\delta D - 8 \cdot \delta^{18}O$ [*Dansgaard*, 1964]. The d excess in oceanic water vapor is a tracer of evaporative conditions (sea surface temperature, surface relative humidity, wind speed) and air-sea interaction [e.g., *Merlivat and Jouzel*, 1979; *Gat*, 1996]. In particular, d excess in water vapor over the ocean increases when humidity over the evaporative ocean decreases, which led *Jouzel et al.* [1982] to interpret isotopic records in polar ice as a tracer of past humidity changes. However, numerous fractionation processes take place along the transport of air masses from the evaporative to the polar regions, so that d excess in ice is also influenced by the moisture source and condensation temperatures, and by the isotopic composition of seawater [*Vimeux*, 1999; *Petit et al.*, 1991; *Stenni et al.*, 2001]. For instance, modeling studies have shown that the effect of relative humidity changes in evaporative regions on polar d excess could be overwhelmed by the effect of sea surface temperature changes at evaporation [*Vimeux*, 1999]. Therefore, d excess is now often interpreted as a tracer of the source temperature [*Vimeux*, 1999; *Stenni et al.*, 2001].

[4] Recent experimental developments have made it possible to accurately measure $H_2^{17}O$ abundance and to define a new isotopic tracer in the water cycle, ^{17}O excess [*Barkan and Luz*, 2007; *Landais et al.*, 2008], expressed in per meg (10^{-3}‰):

$$^{17}\mathrm{O\,excess} = 10^6 \cdot \left(\ln\left(\frac{\delta^{17}O}{1000} + 1\right) - 0.528 \cdot \ln\left(\frac{\delta^{18}O}{1000} + 1\right)\right)$$

[1] LMD, IPSL, UPMC, CNRS, Paris, France.
[2] LSCE, IPSL, CEA, CNRS, UVSQ, Gif-sur-Yvette, France.
[3] UR Great Ice, IRD, LSCE, IPSL, CEA, CNRS, UVSQ, Gif-sur-Yvette, France.

0148-0227/10/2008JD011535

with the δ notation defined as

$$\delta = \left(\frac{R_{\text{sample}}}{R_{\text{SMOW}}} - 1\right) \cdot 1000,$$

where R_{sample} and R_{SMOW} are the molar ratio of the heavy to light isotopes in the sample and in the SMOW standard [*Dansgaard*, 1964]. Note that ^{17}O excess and d excess have slightly different definitions: d excess is defined in a linear scale and ^{17}O excess in a logarithm scale (see *Luz and Barkan* [2005] for the advantage of the logarithm scale).

[5] As δD and δ^{18}O, δ^{17}O and δ^{18}O show different sensitivities to equilibrium and kinetic fractionation processes so that ^{17}O excess, as d excess, has the potential to bring additional information on climate conditions and the hydrological cycle.

[6] The ^{17}O excess and d excess do not show similar spatial distributions and are thus expected to be complementary [*Landais et al.*, 2008]. While d excess in precipitation features a strong poleward gradient over Antarctica [*Dahe et al.*, 1994; *Masson-Delmotte et al.*, 2008], so far ^{17}O excess has shown constant values in present-day Antarctic surface snow [*Landais et al.*, 2008]. Because of these different behaviors, it has been suggested using simple isotopic modeling that ice ^{17}O excess was a more direct tracer of the evaporative regions than ice d excess [*Landais et al.*, 2008].

[7] A record of ^{17}O excess over the last 150 kyr has been obtained from the Vostok ice core (East Antarctica, 78°S, 106°E). The most prominent features are the significant increases of ^{17}O excess by 20 per meg during the last two deglaciations [*Landais et al.*, 2008]. Using a Rayleigh-type distillation model initialized by the traditional closure assumption (i.e., assuming that the vapor originates from surface evaporation only [*Merlivat and Jouzel*, 1979; *Landais et al.*, 2008]) suggested that the large increase in ice ^{17}O excess recorded in the Vostok ice core over the last deglaciation was due to a decrease of relative humidity at the surface (rh_s) by 10 to 20% over the source regions. However, general circulation models (GCMs) suggest very small changes of the near-surface air relative humidity (rh_a) over oceanic regions from LGM to present day [*Bush and Philander*, 1999] or in the context of future climate change [*Bony et al.*, 2006]. If rh_s and rh_a vary in concert, which is assumed in studies interpreting water isotopes in polar ice cores using simple models [*Vimeux et al.*, 2001; *Stenni et al.*, 2001], GCMs simulations contradict the interpretation of ^{17}O excess as a tracer of rh_s.

[8] The goal of this article is thus to explore various processes that might explain the observed glacial-interglacial ^{17}O excess shift, both at the source and during the poleward transport. To this aim, we use a single-column model for tropical or subtropical source regions and a Rayleigh distillation model for the effect along the air mass trajectory, as described and justified in section 2. We explore the effect of source conditions on ^{17}O excess of the moisture source in section 3 and possible modifications of ^{17}O excess between the source and Vostok in section 4. We discuss paleoclimatic implications in section 5.

2. Method

[9] Atmospheric general circulation models (GCMs) incorporating water stable isotopes seem the ideal tool to understand the isotopic composition of worldwide water vapor and precipitation. However, GCMs still have difficulties to simulate surface temperature and snowfall amount over inland Antarctica [*Masson-Delmotte et al.*, 2008]. Moreover, they have difficulties to simulate d excess glacial-interglacial variations of the right sign over high latitudes [e.g., *Werner et al.*, 2001]. This difficulty could arise from either deficiencies in representing isotopic processes such as kinetic effects, or from a poor simulation of some LGM climatic properties influencing d excess, such as surface conditions at the evaporative source. In both cases, these deficiencies reduce the confidence in using GCMs to interpret d excess or ^{17}O excess glacial-interglacial variations in polar ice cores. Consequently, quantitative interpretations of variations in ice d excess are still mainly based on simple Rayleigh distillation models [e.g., *Johnsen et al.*, 1989; *Ciais and Jouzel*, 1994; *Ciais et al.*, 1995; *Kavanaugh and Cuffey*, 2003; *Stenni et al.*, 2001; *Masson-Delmotte et al.*, 2005]. Finally, results from GCMs including $H_2^{17}O$ have not, to our knowledge, been published yet.

[10] To explore processes at work during the transport of air masses from the source regions to the poles, we thus use a Rayleigh type distillation model: MCIM (Mixed Cloud Isotopic Model) [*Ciais and Jouzel*, 1994]. This model permits to quantify the water isotopic fractionation along the air mass trajectory as well as to explore the effect of evaporative recharge over midlatitude and high-latitude oceans (section 4.2).

[11] To represent the influence of source regions on water isotopic composition, most Rayleigh distillation models are initialized by the isotopic composition R_{BL} of an air parcel originating from the planetary boundary layer (BL), and the influences of changing climatic conditions on this isotopic composition are estimated through the so-called closure assumption [*Merlivat and Jouzel*, 1979] (auxiliary material Text S1, section 1)[1]:

$$R_{\text{BL}} = \frac{R_{\text{oce}}}{\alpha_{\text{eq}} \cdot (\alpha_K + \text{rh}_s \cdot (1 - \alpha_K))}, \quad (1)$$

with α_{eq} and α_K the equilibrium and kinetic fractionation coefficients, R_{oce} the isotopic ratios of the ocean surface and rh_s the relative humidity at the surface, i.e., the relative humidity of near-surface air at the temperature of the ocean surface T_s:

$$\text{rh}_s = rh_a \cdot \frac{q_{\text{sat}}(T_a)}{q_{\text{sat}}(T_s)}, \quad (2)$$

where q_{sat} is the specific humidity at saturation and rh_a and T_a are the relative humidity and temperature of the near-surface air, respectively.

[12] The closure assumption relies on the hypothesis that the only source of vapor in the BL is from the surface evaporation (Figure 1a). However, progress in tropical meteorology, in our understanding of the physical processes that control the distribution of water stable isotopes in the atmosphere, and in isotopic modeling, makes the applicability of the closure assumption increasingly questionable [e.g., *Jouzel*

[1] Auxiliary materials are available in the HTML. doi:10.1029/2008JD011535.

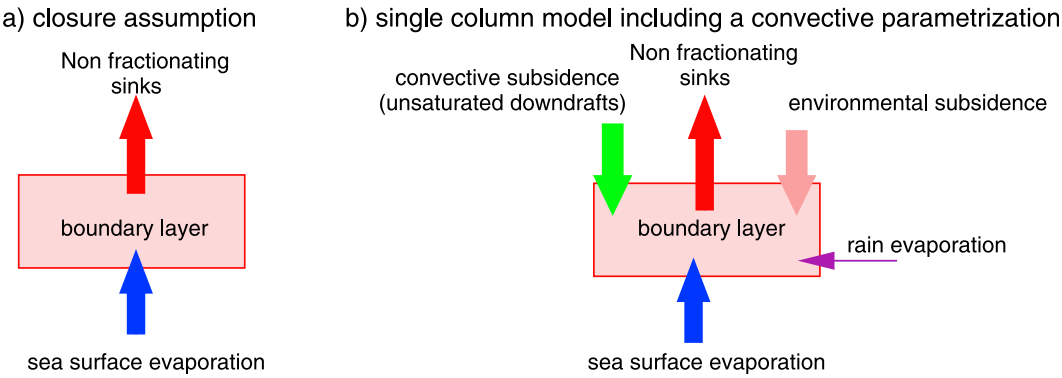

Figure 1. Scheme illustrating the moisture balance of the boundary layer (BL): (a) in the closure assumption [*Merlivat and Jouzel*, 1979] and (b) in the single-column model. Whereas the BL vapor in the closure assumption only originates from sea surface evaporation, the BL vapor in the single-column model receives water vapor from (1) sea surface evaporation (blue), (2) vapor just above the BL, entering the BL through subsiding motions (magenta), (3) unsaturated downdrafts, driven by the rain evaporation (green), and (4) rain reevaporation (purple). In both models the sinks of the BL vapor do not fractionate (e.g., updrafts).

and Koster, 1996; *Delmotte et al.*, 2000]. Besides, in the tropics the BL air is not only influenced by sea surface evaporation but also by convective activity and the large-scale atmospheric circulation [e.g., *Raymond*, 1995]. Observations show that convective processes substantially affect the isotopic composition of the BL vapor [*Lawrence et al.*, 2004]. Large-scale subsidence and boundary layer mixing can also be important in dry regions [*Angert et al.*, 2008]. These reasons may explain why GCMs predict δ^{18}O (d excess) values that can differ from the closure assumption predictions by 3‰ (2‰) in the Tropics and by up to 6‰ (8‰) in mid-latitudes [*Jouzel and Koster*, 1996].

[13] Therefore, to explore the impact on ^{17}O excess of a broader range of processes than those from *Landais et al.* [2008], we use, instead of the closure assumption, a single-column model (SCM) whose physics package incorporates the essential controls of water vapor and water stable isotopes in the tropics and subtropics [*Bony and Emanuel*, 2001]. In particular, the SCM includes the Emanuel convective parametrization [*Emanuel*, 1991], which represents in detail some convective processes such as rain reevaporation and allows for a detailed representation of the isotopic fractionation during these processes [*Bony et al.*, 2008] (Appendix A). The representation by this SCM of cumulus convection and of isotopic processes has been carefully evaluated using tropical data [*Bony and Emanuel*, 2001; *Bony et al.*, 2008]. As illustrated in Figure 1b, in contrast with the closure assumption, the SCM simulates the effect of both large-scale and convective subsidence on the isotopic composition of the BL.

[14] According to GCM studies [*Delaygue et al.*, 2000; *Werner et al.*, 2001], about 15% of the East Antarctic precipitation originates from moisture evaporated in the tropics, 30% from the subtropics (30°S–40°S) and 50% from mid-latitude and high-latitude oceans. The SCM permits to explore the influence of processes (convective processes and large-scale motions in particular) occurring over the Tropics and the subtropics. The 50% of the Vostok precipitation that originates from evaporation in mid and high latitude can be considered as evaporative recharge of air masses during their poleward transport [*Hendricks et al.*, 2000; *Noone*, 2008]. In this paper, we take this recharge into account by adding it to the Rayleigh distillation model. Therefore, the combined analysis of the SCM and MCIM models allows us to consider the main processes that are likely to affect the isotopic composition of the polar snowfall: conditions at the evaporative source (surface conditions, convection), Rayleigh distillation and evaporative recharge over mid and high latitudes. Note that the condensation in frontal clouds is represented in a simple and implicit way by the Rayleigh distillation of MCIM. This latter does not allow to represent the impact, on the isotopic composition of the water transported poleward, of changes that might occur in the physical or microphysical properties of frontal cloud systems during climate change.

3. Single-Column Simulation of the Isotopic Composition of the Vapor Evaporated From the Tropics and Subtropics

[15] The single-column model and its isotopic implementation were extensively described by *Bony and Emanuel* [2001] and *Bony et al.* [2008], and are summarized in Appendix A. Each of our SCM simulation represents the steady state of the atmosphere in radiative-convective equilibrium, determined by the boundary conditions: surface temperature and wind speed, large-scale profile of vertical velocity, radiation, CO_2. The model is ran over tropical and subtropical oceanic conditions.

[16] For example, for a wind speed of 5 m/s, sea surface temperature of 25°C and no large-scale ascent or descent (corresponding to average tropical conditions), the precipitation rate is about 3.6 mm/d and the simulated isotopic composition of the BL vapor is −12.9‰, 14.7‰ and 20 per meg for δ^{18}O, d excess and ^{17}O excess, respectively. These values compare well with measurements over tropical ocean: δ^{18}O $\simeq$ −10‰ to −13‰ [*Lawrence et al.*, 2004]. Very few data are available for d excess and ^{17}O excess in tropical oceanic vapor. For comparison, unpublished results over the Amazon are in the ranges of 10–20‰ for d excess and 15–20 per meg for ^{17}O excess.

Table 1. Isotopic Composition of the Source Vapor and Vostok Ice Simulated by the SCM and MCIM Depending on Boundary at the Vapor Source[a]

Sensitivity Test	V_s (m/s)	SST (°C)	ω (hPa/d)	P (mm/d)	δ^{18}O in BL (‰)	d in BL (‰)	^{17}O Excess in BL (per meg)	δ^{18}O if Closure (‰)	d if Closure (‰)	^{17}O Excess if Closure (per meg)	rh$_a$ (%)	rh$_s$ (%)	δ^{18}O in Ice (‰)	d in Ice (‰)	^{17}O Excess in Ice per meg)
Control	5	25	15	1.4	−12.1	14.4	19.3	−10.5	12.9	16.2	78.8	71.2	−54.2	15	42
SST	5	21	15	2.3	−11.9	11.3	12.4	−10.7	10.2	12.9	80.7	74.6	−51.9	8.3	34
SST	5	29	15	2.6	−11.6	15.2	18.9	−10.1	13.6	16.0	79.9	72.1	−53.3	17.5	40
V_s	2	25	15	1.3	−13.3	20.9	24.8	−11.3	18.7	27.9	69.3	57.6	−53.4	20.2	49
V_s	3	25	15	1.7	−12.9	18.2	23.7	−11.0	16.1	22.9	73.2	63.5	−53.5	19.1	48
V_s	6.5	25	15	2.6	−11.6	12.5	15.3	−10.3	11.2	12.7	80.7	75.1	−53.0	13.6	39
ω_{max}	5	25	30	0.5	−10.5	10.9	8.2	−10.2	10.5	11.31	81.8	76.8	−52.9	8.3	31
ω_{max}	5	25	0	3.6	−12.9	14.7	19.8	−10.6	13.4	17.2	77.7	70.6	−53.3	15.7	44
ω_{max}	5	25	−30	6.9	−15.2	19.8	27.0	−10.9	15.5	21.5	73.8	65.0	−54.9	21.7	50
ω_{max}	5	25	−60	9.8	−16.7	22.3	28.1	−11.0	16.4	23.4	71.9	62.8	−56.1	27.2	52
ω_{max}	5	25	−90	12.4	−17.9	24.9	28.9	−11.1	17.4	25.4	70.0	60.5	−56.8	31.5	53

[a]Boundary conditions imposed to the SCM: surface wind speed V_s, sea surface temperature SST, and large-scale circulation ω (the large-scale vertical velocity at 500 hPa; negative values indicates large-scale ascent). Also given are precipitation rate P, isotopic composition of the boundary layer (BL) (δ^{18}O, d excess d, and ^{17}O excess), isotopic composition of the BL if it was predicted by the closure assumption [*Merlivat and Jouzel*, 1979], relative humidity of the air at the lowest-level rh_a and relative humidity at the surface rh_s, simulated at equilibrium by the single-column model. The humidity rh_s is calculated using equation (2). Finally, isotopic composition of the ice simulated by the MCIM (see section 5.1) for the different initial conditions given in the previous columns are shown in columns δ^{18}O, d, and ^{17}O excess. Control entries are for the control simulation described in section 4.1.

[17] Compared to the closure assumption, the SCM yields δ^{18}O 2.3‰ lower, d excess 1.3‰ higher and ^{17}O excess 3 per meg higher (Table 1), in agreement with GCM outputs [*Jouzel and Koster*, 1996]. In the SCM, this is due to the admixture into the BL of depleted and high d excess vapor by the unsaturated downdraft (Figures 1 and 2). Therefore, considering convective downdrafts in the SCM leads, in regions of significant convection, to a significant modification of the BL composition compared to the closure assumption.

3.1. Sensitivity to Boundary Conditions

[18] To investigate what controls the BL composition in the SCM, we perform sensitivity tests to large-scale boundary

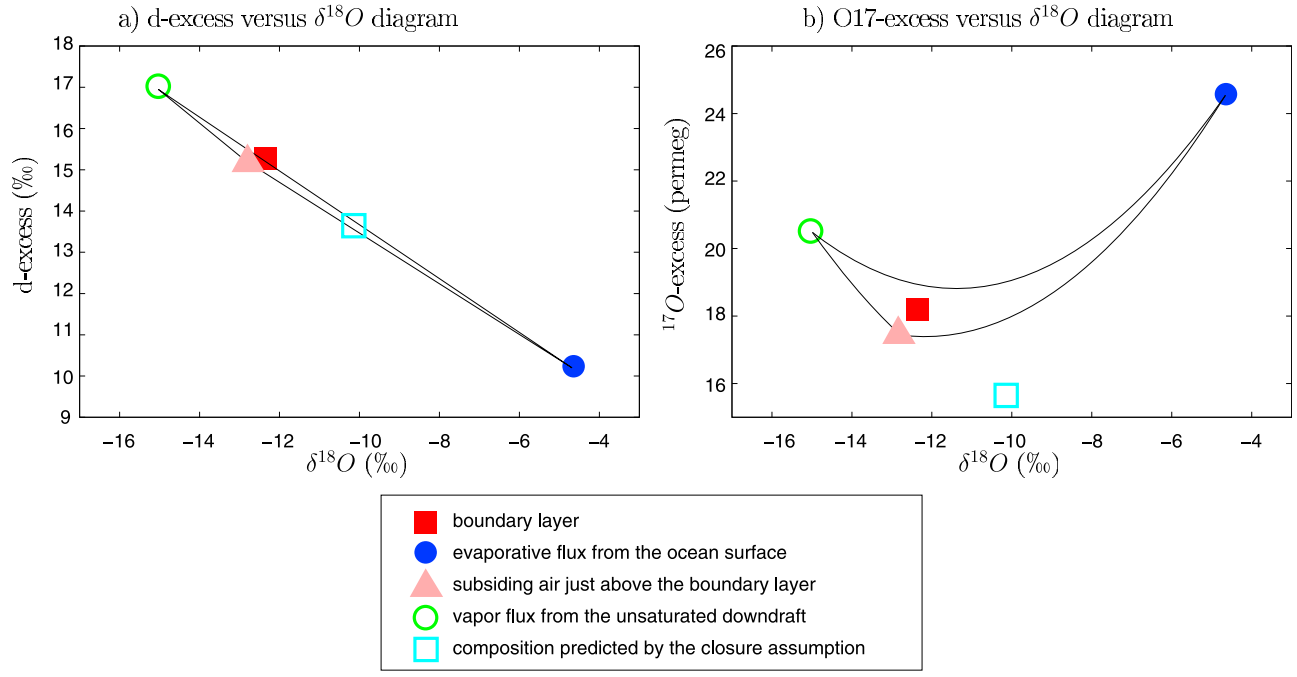

Figure 2. Isotopic composition of the BL simulated by the model (red solid square) in δ^{18}O versus (a) d excess and (b) ^{17}O excess diagrams. The composition of the unsaturated downdraft vapor mass flux into the boundary layer, the evaporative flux from the ocean, and the subsiding environment just above the boundary layer are shown with green open circles, blue solid circles, and magenta solid triangles, respectively. Mixing lines (lines representing the ensemble of possible mixtures between two samples) are in black. The isotopic composition of the boundary layer predicted by closure assumption for the simulated surface conditions is shown with cyan open squares.

conditions: sea surface temperature (SST), surface wind speed and large-scale vertical velocity at 500 hPa (ω, controlling the convective intensity). Note that the surface relative humidity (rh_s) is not a boundary condition in the model, but rather a prognostic variable that depends mainly on the surface wind speed and on the large-scale convective activity.

[19] All sensitivity tests are performed around a control simulation corresponding to subtropical/tropical conditions (45% of the moisture source according to GCMs), with an SST of 25°C, surface wind speed of 5 m/s and a large-scale descent of 15 hPa/d at 500 hPa. We vary the boundary conditions of the SCM within a range for which the neglect of horizontal advections constitutes a reasonable approximation: SST from 21°C to 24°C, wind speed from 2 to 6.5 m/s and vertical velocity from −90 to +30 hPa/d.

[20] Note that we test independently the sensitivity to SST, surface wind and large-scale velocity to better isolate their effects, though in nature these variables vary in concert [*Sobel and Bretherton*, 2000; *Bony et al.*, 2004].

3.1.1. Sensitivity to SST

[21] We test SST variations of up to 4°C, which is an upper bound of SST glacial-interglacial variations at low latitudes [*Harrison*, 2000; *Barrows and Juggins*, 2005; *Waelbroeck et al.*, 2009]. The sensitivity to SST simulated by the SCM is of 0.08 ‰/°C for δ^{18}O and 0.3‰/°C in d excess (Figure 3a, red solid line and Table 1). This sensitivity is predicted by the closure assumption (Figure 3a, dotted green line) and is due mainly to the variation of fractionation coefficients with temperature.

[22] The BL ^{17}O excess is not expected to change with temperature [*Barkan and Luz*, 2005]. Indeed, $\frac{\ln(^{17}\alpha_{eq})}{\ln(^{18}\alpha_{eq})}$ remains equal to 0.529 for temperature variations between 10°C and 40°C (with $^{17}\alpha_{eq}$ and $^{18}\alpha_{eq}$ the fractionation coefficients at liquid-vapor equilibrium for $H_2^{17}O/H_2^{16}O$ and $H_2^{18}O/H_2^{16}O$). The 7 per meg increase in ^{17}O excess from 21°C to 25°C (Figure 3a) is only due to the 3% decrease in rh_s (driving a 3 per meg increase in ^{17}O excess) and the 1 mm/d increase in precipitation (driving a 4 per meg increase in ^{17}O excess). These sensitivities to rh_s and precipitation will be explained in sections 3.1.2 and 3.1.3.

3.1.2. Sensitivity to Surface Wind Speed

[23] We vary the surface wind speed V_s along a range of values typically found over tropical oceans from 2 to 6.5 m/s. We only test values in the smooth regime below 7 m/s (where the kinetic fractionation is constant), since 95% of the ocean surface is in this regime [*Eriksson and Bolin*, 1964]. Besides, V_s greater than 7 m/s would imply a large change in the kinetic fractionation coefficient at the transition between smooth and rough regime [*Merlivat and Jouzel*, 1979], whose physical significance over the ocean remains unclear.

[24] As V_s increases, δ^{18}O increases (0.9 ‰/(m/s)) and both d excess and ^{17}O excess decrease (−2.4‰/(m/s) and −4.4 per meg/(m/s), respectively: Figure 3b, solid red line). The sensitivity of the isotopic composition to V_s is mainly explained by coincident rh_s variations: when V_s increases, surface evaporation is enhanced, the water content in the BL increases and rh_s increases, by about 4.6%/(m/s) (Figure 4b). To quantify the effect of rh_s, we performed the same simulations but with rh_s artificially fixed constant at 70% in the calculation of the isotopic composition of the evaporation flux. Without the coincident variations in rh_s, the sensitivity of the isotopic composition to V_s becomes very small (Figure 4b, dotted green line), confirming that the underlying factor explaining this sensitivity is rh_s.

3.1.3. Sensitivity to Convective Intensity

[25] Convective intensity is modulated in the SCM by prescribing a large-scale ascent or descent within the troposphere, and measured by the precipitation rate P.

[26] BL vapor δ^{18}O decreases by about 0.4 ‰/(mm/d) as convective intensity increases (Figure 3d), consistent with the well-known tropical amount effect observed in the precipitation [*Dansgaard*, 1964; *Rozanski et al.*, 1993]. This compares well with the measurements of *Lawrence et al.* [2004] over tropical ocean ranging from −10‰ in quiescent weather to below −20‰ after intense convective systems. Meanwhile, d excess increases by about 0.6‰/(mm/d) as convective intensity increases (Figure 3c, solid red line).

[27] Convective processes decrease δ^{18}O and increase d excess in the BL vapor mainly through convective mixing bringing down depleted and high d excess vapor [*Risi et al.*, 2008]. However, as for the sensitivity to V_s, part of the sensitivity of d excess to convection is explained by coincident rh_s variations: convection dries the BL in the model, owing to stronger upward transport of humidity by convective fluxes. Sensitivity tests to convective intensity in which rh_s is artificially held constant at 70% in the calculation of the composition of the surface evaporation (Figure 3c, dotted green line) show that the effect of rh_s contributes for 55% to the sensitivity to convection. This explains why the closure assumption partly predicts the effect of rh_s on the BL d excess, despite its neglect of convective processes (Figure 3c, dashed blue line).

[28] The ^{17}O excess increases with increasing convective activity by about 0.8 per meg/(mm/d) as precipitation increases from 4 mm/d to 12 mm/d (Figure 3c). For these precipitation rates, the increase in ^{17}O excess is mainly due to the decrease in rh_s: without coincident rh_s variations, the BL ^{17}O excess varies by less than 0.1 per meg/(mm/d) (dotted green line).

Figure 3. Thick red line denotes sensitivity of boundary layer δ^{18}O, d excess, and ^{17}O excess to (a) sea surface temperature (SST), (b) surface wind speed, and (c) convective intensity, measured here as precipitation rate. Dashed blue line denotes sensitivity predicted by closure assumption for the same SST and the same relative humidity at the surface. Dotted green line denotes sensitivity simulated by the model when the relative humidity at the surface is held artificially constant at 70% in the calculation of the composition of surface evaporation, highlighting the direct effect of convective processes on the BL composition (sections 3.1.2 and 3.1.3). The gray shading represents the envelope of the simulated boundary layer compositions (δ^{18}O, d excess, and ^{17}O excess) when model parameters related to unsaturated downdraft are varied by ±20% and when parameter ϕ is varied from 0 to 0.9. (d) Sensitivity to rh_s, deduced from the sensitivity tests, to V_s (solid pink line) and convective activity (dashed pink line); the simulations with "constant" rh_s have been subtracted from the standard simulations to isolate the effect of rh_s. Also shown is the closure assumption (dashed blue line).

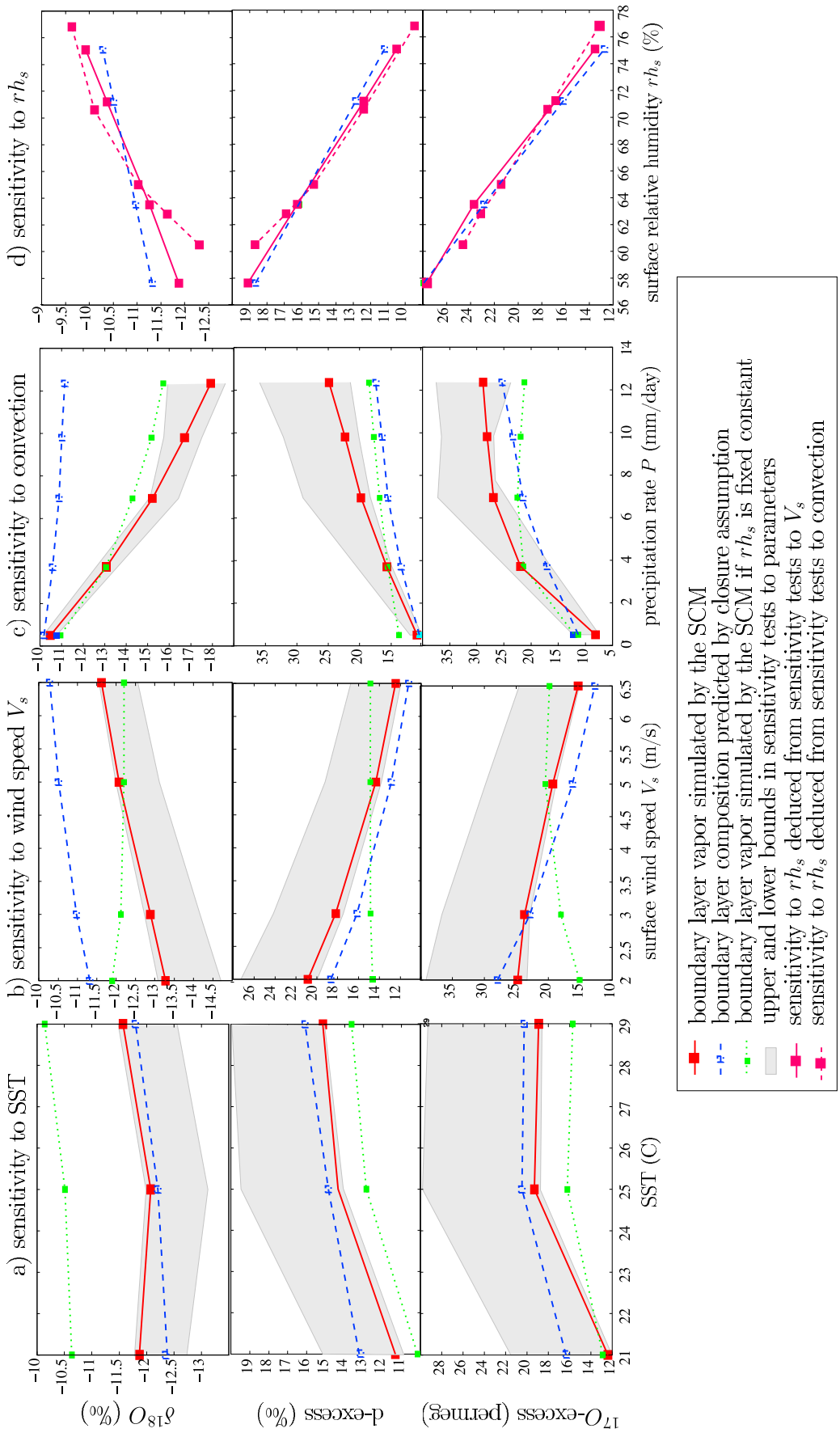
a) sensitivity to SST
b) sensitivity to wind speed V_s
c) sensitivity to convection
d) sensitivity to rh_s
$\delta^{18}O$ (‰)
d-excess (‰)
^{17}O-excess (permeg)
SST (C)
surface wind speed V_s (m/s)
precipitation rate P (mm/day)
surface relative humidity rh_s (%)
boundary layer vapor simulated by the SCM
boundary layer composition predicted by closure assumption
boundary layer vapor simulated by the SCM if rh_s is fixed constant
upper and lower bounds in sensitivity tests to parameters
sensitivity to rh_s deduced from sensitivity tests to V_s
sensitivity to rh_s deduced from sensitivity tests to convection

Figure 3

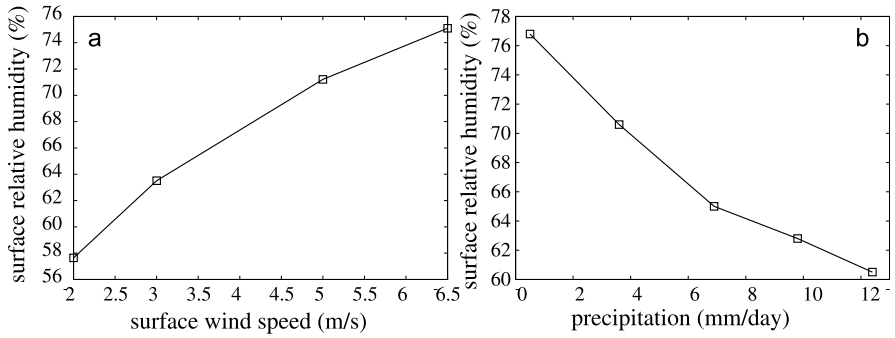

Figure 4. Sensitivity of surface relative humidity rh_s to (a) surface wind speed V_s and (b) precipitation in the SCM simulations. In Figure 4a, SST = 25°C, ω_{max} = 15hPa/d, and V_s is varied from 2 to 6.5 m/s. In Figure 4b, SST = 25°C, V_s = 5m/s, and ω_{max} is varied from −90 to 30hPa/d.

The sensitivity of ^{17}O excess to convective activity is higher for low precipitation rate: 4 per meg/(mm/d) for precipitation rates lower than 4 mm/d. Variations in rh_s account for 40% of this sensitivity for these precipitation rates.

3.2. Main Drivers of ^{17}O Excess Changes in the Source Regions

[29] The previous experiments have revealed that convective processes and changes in rh_s were the two main processes underlying the sensitivities of ^{17}O excess to boundary conditions.

[30] To calculate an upper bound for the impact of convective processes on ^{17}O excess, we assume that the precipitation rate varies from 1 mm/d at LGM to 4 mm/d at EH in tropical and subtropical regions contributing to 50% of the Vostok precipitation. This is an extreme assumption since (1) GCMs rarely simulate larger precipitation changes, even regionally [*Braconnot et al.*, 2007], (2) tropical and subtropical regions are not expected to contribute more than 50% to the Vostok precipitation [*Delaygue et al.*, 2000] and (3) the sensitivity to convection is maximum at low precipitation rates. Excluding the effect of coincident rh_s variations, this would lead to a change of only 4 per meg in the Vostok precipitation, thus explaining 20% of the observed ^{17}O excess change. Convection is therefore a minor influence on ice ^{17}O excess.

[31] Sensitivity experiments to V_s and convection have revealed the large influence of rh_s on ^{17}O excess. By comparing the sensitivity to V_s with and without fixed rh_s (Figure 3d, solid pink line), we estimate the sensitivity of ^{17}O excess to rh_s to −1.0 per meg/%. Similarly, the δ^{18}O and d excess sensitivities to rh_s are 0.2‰/% and −0.5‰/%.

[32] These sensitivities to rh_s are roughly linear (Figure 3d). and consistent both with the closure assumption (dotted green line) and with the sensitivities deduced from the response to convection (dashed pink line), supporting the robustness of these sensitivities to rh_s. We thus suggest that these sensitivities to rh_s are robust and can be applied in extratropical conditions as well, as suggested also by d excess and ^{17}O excess observations over midlatitude and high-latitude Southern Ocean [*Uemura et al.*, 2008, 2010].

[33] Taking into account uncertainties in the ^{17}O excess sensitivity to rh_s (auxiliary material Text S1, section 2), a 12 to 22% decrease in rh_s from LGM to EH may explain the 20 per meg change in BL ^{17}O excess, a conclusion similar to that of *Landais et al.* [2008].

4. Poleward Transport Processes

[34] To understand how ^{17}O excess variations in the source regions are transmitted to d excess and ^{17}O excess in the polar regions, we initialize the MCIM with the BL isotopic composition simulated by the SCM (section 3) and simulate the isotopic composition of the snowfall over the Vostok station (−55°C, 3500 m above sea level [*Petit et al.*, 1999]). Table 1 displays δ^{18}O, d excess and ^{17}O excess simulated in the ice at the Vostok location. The δ^{18}O, d excess and ^{17}O excess simulated by the model (−54.2‰, 17.5‰ and 40 per meg, respectively) compare reasonably well with the measurements in Vostok for the present day (about −55‰, 16‰ and 40 per meg, respectively, for annual averages). Nevertheless, an accurate simulation of the Vostok snowfall composition is not expected given the idealized framework of both the SCM and MCIM. We thus focus here on the sensitivity to climatic conditions rather than the absolute value of the isotopic composition.

4.1. Effect of Pure Rayleigh Distillation

[35] The sensitivities of d excess and ^{17}O excess in the source BL to source conditions is also visible in the polar snowfall isotopic composition (Table 1). For example, when increasing rh_s from 69 to 81%, d excess and ^{17}O excess decrease both in the source BL and in the polar snowfall. However, distillation processes induce a dampening of the initial vapor d excess anomaly: while ^{17}O excess decreases by 10 per meg both in the source vapor and in the snowfall, d excess decreases by 8.4‰ in the source vapor and only by 6.6‰ in the surface snow. Here are two reasons for these different behaviors of d excess and ^{17}O excess along the distillation process.

[36] 1. A change in δ^{18}O of the source vapor influences d excess in the snowfall even if the source d excess remains constant [e.g., *Delaygue*, 2000; *Cuffey and Vimeux*, 2001; *Werner et al.*, 2001; *Vimeux et al.*, 2002; *Jouzel*, 2003]. On the contrary, ^{17}O excess is not affected by such a change in δ^{18}O of the source region (Table 2, last two rows), due to the different definitions of d excess (linear) and ^{17}O excess (logarithm) (auxiliary material Text S1, section 3).

Table 2. Isotopic Composition of the Ice Simulated for Different Source and Site Temperatures and Different δ^{18}O of the Boundary Layer[a]

T_{source} (°C)	T_{site} (Inversion) (°C)	Vapor δ^{18}O (‰)	Ice δ^{18}O (‰)	Ice d Excess (‰)	Ice ^{17}O Excess (‰)
26	−35	−13	−55.6	27.5	42
24	−35	−13	−54.5	24.5	42
28	−35	−13	−56.8	30.6	43
26	−38	−13	−59.6	35	43
26	−32	−13	−51.6	21	42
26	−35	−10	−52.7	20	42
26	−35	−16	−58.5	35	42

[a]In the boundary layer, d excess is 15‰ and ^{17}O excess is 20 per meg.

[37] 2. The d excess is influenced by air temperature while ^{17}O excess is almost insensitive to temperature along the distillation (Table 2, first three rows), due to different evolutions of the equilibrium fractionation coefficients with temperature. Indeed, while $\frac{\ln(^{17}\alpha_{eq})}{\ln(^{18}\alpha_{eq})}$ remains equal to 0.529 for temperature increasing from 0°C to 20°C, $\frac{^{D}\alpha_{eq}-1}{^{18}\alpha_{eq}-1}$ varies between 9.6 and 8.7 ($^{D}\alpha_{eq}$ being the fractionation coefficient at liquid-vapor equilibrium for $HD^{16}O/H_2^{16}O$). Note that a similar dependency on temperature is observed for $\delta D/\delta^{18}O$ if we consider the evolution of $\frac{\ln(^{D}\alpha_{eq})}{\ln(^{18}\alpha_{eq})}$ (9.1 at 0°C and 8.4 at 20°C) and the same behavior holds for vapor-solid fractionation. Therefore, the near-surface temperature in the moisture source regions influences the polar snowfall d excess [*Petit et al.*, 1991; *Vimeux et al.*, 2002] but not ^{17}O excess.

[38] Consequently, the ^{17}O excess variations of the BL vapor in the source region are perfectly preserved in the polar precipitation (Table 2). On the contrary, the polar d excess is sensitive to the initial and final temperatures of the distillation (Table 2), and thus only partially reflects the d excess signal from the source region.

4.2. Effect of Evaporative Recharge

[39] Classical Rayleigh distillation models assume that air parcels are isolated. However, in nature, air masses are partially recharged through surface evaporation: for example, *Trenberth* [1998] estimated a recycling ratio (proportion of the moisture originating from the local evaporation versus horizontal advection) from 10 to 20% at the 1000 km scale over subtropical and midlatitude oceans. The isotopic composition of Antarctic snowfall is affected by the evaporative recharge [*Kavanaugh and Cuffey*, 2003; *Lee et al.*, 2008] and the competition between mixing of surface evaporated water through the BL and poleward advection of moisture [*Noone*, 2008]. Evaporative recharge is expected to affect even more strongly ^{17}O excess than δ^{18}O or d excess because mixing lines are curved in a logarithmic plot (Figure 5a), so that ^{17}O excess is not preserved during mixing.

[40] To quantify the effect of evaporative recharge through the mixing of air masses with contrasted δ^{18}O, we perform an idealized sensitivity experiment. We start a distillation of the initial vapor (δ^{18}O = −12 ‰, d excess = 15‰, ^{17}O excess = 18 per meg) until the vapor reaches a 2‰ δ^{18}O depletion. Then, we recharge 10% of the vapor by an evaporative source, corresponding to the composition of the evaporation flux simulated by the SCM in the control simulation: δ^{18}O = −5‰ (consistent with *Lee et al.* [2007]), d excess = 10‰, ^{17}O excess = 25 per meg (Figure 2). The same distillation-recharge steps are repeated again until the precipitation δ^{18}O corresponds to the δ^{18}O measured at the coast of Antarctica. Then, the parcel is distilled without recharge until reaching the Vostok station. This experiment is roughly equivalent to a recycling ratio of 20% at the 1000 km scale (consistent with *Trenberth* [1998], until 70°S in latitude. Compared to an isolated parcel, ^{17}O excess in Vostok snowfall is lower by 14 per meg, due to the curvature of the mixing lines (Figure 5). The Vostok snowfall d excess is just slightly reduced by 4‰ due to the admixture of lower d excess vapor by surface evaporation.

[41] Note that recycling in this test is artificial and does not accurately represent the complexity of recharge processes. Also, this test estimates an upper bound of the effect by mixing the distilled air mass with a very contrasted δ^{18}O. If the vapor was recharged with a less contrasted vapor (δ^{18}O = −12‰ instead of −5‰, for example, recharge by vertical mixing with the BL [*Noone*, 2008], the Vostok ^{17}O excess would be lower by 10 per meg instead of 14 per meg. The recycling ratio used is also an upper bound, since air masses in mid and high latitudes are not transported poleward directly in contact with the ocean surface [*Noone*, 2008].

[42] Finally, we find a maximum sensitivity of ^{17}O excess to the evaporative recycling ratio of −0.7 to −0.5 per meg/%. A decrease of the recycling ratio from LGM to EH by 30% to 40% (i.e., recycling ratio from 40–60% to 10–20%) would thus be required to explain by itself the 20 per meg ^{17}O excess increase. For the LGM to present-day change, PMIP2 models [*Braconnot et al.*, 2007] simulate a slight decrease (smaller than 5%) of the recycling ratio between 20°S and 60°S from LGM to present day. This process is thus not likely to contribute to more than 20% to the observed ^{17}O excess increase from LGM to EH.

4.3. Effect of δ^{18}O Seasonality in Antarctica

[43] Due to the curvature of the mixing lines in the log-log diagram, the annually averaged ^{17}O excess in precipitation depends on the amplitude of the δ^{18}O seasonal cycle (Figure 5b): if the seasonal amplitude of δ^{18}O in snowfall increases, then the annually averaged ^{17}O excess decreases. As an example, we assume that at present day, 40% of the Vostok snow accumulation occurs from October to March with a δ^{18}O of −50‰ and that the remaining 60% of the accumulation occurs from April to September with a δ^{18}O of −60‰ (values of the same magnitude as reported by *Ekaykin* [2003]). For simplicity, we assume a constant ^{17}O excess in the snowfall all over the year. If the seasonal amplitude of δ^{18}O in Vostok snowfall increases from 10‰ today to 20‰ during the LGM, then the annual ^{17}O excess in Antarctica snowfall decreases by 10 per meg (Figure 5b). Since mixing lines are linear when dealing with d excess, this last effect does not affect the d excess.

[44] No data describing δ^{18}O seasonality in Antarctica are available during the LGM. Some isotopic GCM show either no change [*Jouzel et al.*, 1994] or a small change (20% in simulations presented by *Jouzel et al.* [2007b]) in the seasonal cycle in Eastern Antarctica between the LGM and today. PMIP2 models simulate a decrease of the seasonal amplitude of temperature from LGM to present day, ranging from about 0°C to 6°C over Antarctica depending on

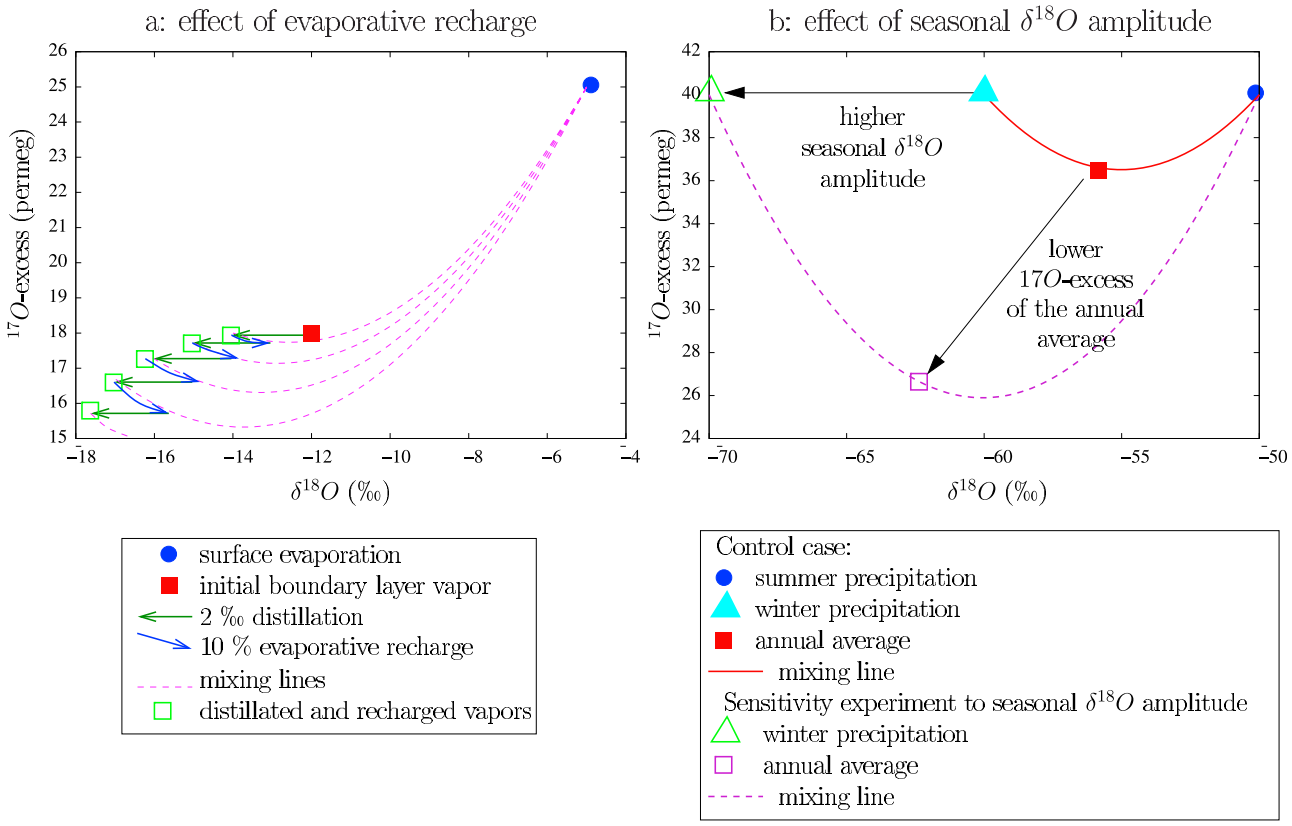

Figure 5. Schemes illustrating the effect of (a) the evaporative recharge of air masses along their poleward transport and (b) the seasonal amplitude of snow δ^{18}O over Antarctica. Both effects are due to the curvature of the mixing lines in the ^{17}O excess versus δ^{18}O diagram, because of the logarithmic definition of ^{17}O excess. In Figure 5a, in an idealized sensitivity experiment to evaporative recharge described in section 4.2, an initial boundary layer vapor (solid red square) undergoes successive distillation and recharge steps by a surface evaporation flux (blue circle). Both the initial vapor and surface evaporation have the composition illustrated on Figure 2. As the distillation depletes the vapor without significantly changing its ^{17}O excess, evaporative recharge decreases ^{17}O excess due to the curvature of the mixing lines. In Figure 5b, in an idealized sensitivity experiment, we assume that at the present day, 40% of the Vostok snow accumulation occurs from October to March with a δ^{18}O of −50‰ and the remaining 60% of the accumulation occurs from April to September with a δ^{18}O of −60‰ (values of the same magnitude as reported by *Ekaykin* [2003]). If the amplitude of the δ^{18}O seasonal cycle in Antarctic snow is increased from 10‰ to 20‰, then the annual ^{17}O excess of the snow decreases by about 10 per meg, due to the curvature of the mixing line.

models. We thus propose here a rough estimate based on temperature seasonality derived from GCM simulations of the LGM, and applying the modern seasonal slope of $\frac{d\delta^{18}O}{dT}$ 0 ~ 4‰/*K* [*Ekaykin and Lipenkov*, 2008]. As an upper bound for this effect, considering a decreased seasonal amplitude of 6°C from LGM to EH, the δ^{18}O seasonal amplitude in polar snowfall would decrease by 2.4‰ from LGM to EH. The consequence is a small increase of snowfall ^{17}O excess of about 2.4 per meg from LGM to EH.

[45] Given these results, the variation in the seasonality of δ^{18}O is thus unlikely to contribute for more than 15% to the observed ^{17}O excess shift.

5. Paleoclimatic Implications

[46] In sections 3 and 4, we have explored different processes affecting the source ^{17}O excess, its evolution along air mass distillation and the impact of precipitation seasonality. While convective changes, recharge and seasonality may account for part of the ^{17}O excess shift between the LGM and EH, these influences, even combined, are not likely account for more than 50% of the shift. On the other hand, a higher rh_s at LGM by 12 to 20%, would explain the observed shift (as in work by *Landais et al.* [2008]). This is an upper bound, neglecting the role of the aforementioned processes that have a secondary impact. We discuss here the realism of an extreme 20% change in rh_s and its implications for LGM temperature reconstructions using stable water isotopes in ice cores.

5.1. Realism of a Higher rh_s Over Evaporative Regions During the LGM

[47] As mentioned in section 1, GCMs outputs do not produce significant changes of rh_a between the LGM and the present day [*Bush and Philander*, 1999] thus questioning the interpretation of the ^{17}O excess shift. However, variations

in rh_s are not equal to variations in rh_a. The rh_s differs from rh_a owing to the difference between the air and surface temperatures (thermodynamic disequilibrium) [*Angert et al.*, 2008; *Pfahl and Wernli*, 2008]. By differentiating equation (2) as a function of rh_a, T_s and T_s-T_a, and quantifying the different terms for rh_a ranging from 60 to 80%, T_s from 0°C to 15°C (conditions over midlatitude oceans, which are important sources of the Vostok precipitation) and T_s-T_a from −3°C to 3°C, we express the variations of rh_s as

$$\Delta rh_s = (1.0 \pm 0.2) \cdot \Delta rh_a - (2 \pm 11) \cdot 10^{-2} \cdot \Delta T_s - (4.7 \pm 0.7) \cdot \Delta(T_s - T_a). \quad (3)$$

[48] Variations in rh_s can thus arise either from a variation of rh_a of the same order of magnitude (first term on the right-hand side) or a variation in the thermodynamical disequilibrium between the sea surface and the near-surface air T_s-T_a (third term). The second term is negligible (ΔT_s of 10°C yields rh_s variations lower than 1%).

[49] A first possibility to explain the rh_s decrease from LGM to EH is a decrease of rh_a over the source region. This can be obtained through a general rh_a decrease over the Indian and Southern oceans or through a shift of the location of the moisture sources toward regions of lower relative humidity. On the one hand, PMIP2 simulations show variations lower than 3% between 20°S and 60°S. Moreover, GCMs simulate a poleward shift of the source regions from LGM to EH [*Delaygue et al.*, 2000; *Werner et al.*, 2001], which is not consistent with a decrease in rh_a from LGM to EH, since rh_a increases poleward [*Vimeux et al.*, 2001].

[50] On the other hand, *Jouzel et al.* [1982] argued that a higher rh_a during the LGM could be consistent with higher wind speeds over the ocean during this period, as suggested by highest aerosol and sea salt content measured in Antarctic ice [*Petit et al.*, 1981, 1999]. In addition, global warming during the deglaciation are associated with a change in the intensity, frequency and latitudinal position of the storm tracks [*Laîne et al.*, 2008; *Toggweiler et al.*, 2006] and with a southward shift of the Intertropical Convergence Zone during the LGM [*Chiang and Bitz*, 2005; *Kang et al.*, 2008]. Such large reorganizations could also affect the latitudinal distribution of relative humidity at low levels.

[51] A second possibility to explain the variations of rh_s is a change in the thermodynamical disequilibrium between the sea surface and the near-surface air in the source regions (equation (3)). For example, the 20% higher rh_s during the LGM could be explained by a 4°C lower T_s-T_a (i.e., T_s increase from LGM to EH 4°C more strongly than T_a). However, LGM simulations with coupled ocean-atmosphere models conducted in PMIP2 [*Braconnot et al.*, 2007] do not show such a disequilibrium. They rather simulate a slightly lower rh_s (decrease of 3% in average between 30°S and 60°S) during the LGM.

[52] There is thus a mismatch between the 20% change in rh_s suggested by the ^{17}O excess shift in polar ice and the small variations in rh_s simulated by GCMs.

5.2. Implications of Relative Humidity Changes on LGM Temperatures Reconstructions

[53] If true, a large change in surface relative humidity at the source may have strong consequences for the classical interpretation of ice δ^{18}O and d excess as indicators of site and source temperatures T_{site} and T_{source} [*Vimeux et al.*, 2002; *Jouzel et al.*, 2007a; *Masson-Delmotte et al.*, 2005; *Stenni et al.*, 2001]. Indeed, δ^{18}O and d excess in polar snowfall also depend on the variations in rh_s in the source regions. Until now, variations in rh_s were assumed to equal variations in rh_a, and variations in rh_a were either neglected or assumed to vary with T_{source} by −0.38‰/°C [*Vimeux et al.*, 2002]. This slope was obtained from spatial correlation between SST (between 7°C and 24°C) and rh_a from GCM outputs for present-day simulations [*Vimeux et al.*, 2002]. However, these assumptions are questionable: (1) rh_s can vary even though rh_a is constant and (2) seasonal correlations between SST and rh_a in NCEP data [*Kalnay et al.*, 1996] show weak values and variations in sign, questioning whether the slope given by *Vimeux et al.* [2002] is robust and holds in time (especially between glacial and interglacial periods). Therefore, changes in rh_s might have been underestimated in previous studies.

[54] In the light of the rh_s variations suggested by the ^{17}O excess record, we thus reconsider the previous temperature reconstructions in Vostok over the deglaciation based on δ^{18}O and d excess records alone. To do so, we perform an inversion of the δ^{18}O and d excess ice core data at LGM to retrieve simultaneously T_{site} and T_{source}. The system of equations for δ^{18}O and d excess in ice are derived from MCIM simulations initialized by the SCM (Table 1), assuming linear relationships:

$$\Delta\delta^{18}O_{corr\,SW} = -0.30 \cdot \Delta T_{source} + 1.0 \cdot \Delta T_{site} + 0.02 \cdot \Delta rh_s \quad (4)$$

$$\Delta d_{corr\,SW} = 1.50 \cdot \Delta T_{source} - 1.1 \cdot \Delta T_{site} - 0.38 \cdot \Delta rh_s \quad (5)$$

where $\Delta\delta^{18}O_{corr\,SW}$ and $\Delta d_{corr\,SW}$ are the variations of δ^{18}O and d excess in the Vostok ice from LGM to EH, corrected by the −1 ‰ change in seawater δ^{18}O from LGM to EH: $\Delta\delta^{18}O_{corr\,SW}$ = +7‰ and $\Delta d_{corr\,SW}$ = +1 ‰ [*Jouzel*, 2003].

[55] The coefficients for the sensitivity of Vostok $\Delta\delta^{18}$O and Δd to ΔT_{source} and ΔT_{site} are given with a 20% uncertainty and are similar to those obtained by *Vimeux et al.* [2002] except for (1) $\frac{\partial d}{\partial rh_s}$: −0.15‰/% in work by *Vimeux et al.* [2001] and −0.38‰/% in this study, and (2) $\frac{\partial d}{\partial T_{site}}$: −0.5‰/*K* in work by *Vimeux et al.* [2002] and −1.1‰/*K* in this study, due to a different tuning of the MCIM (mainly supersaturation parametrization) based on the additional constraint from ^{17}O excess [*Landais et al.*, 2008].

[56] Doing the extreme assumption that the increase in ^{17}O excess from LGM to EH should be attributed to a decrease in rh_s only, we have Δrh_s = −20% and obtain ΔT_{site} = +7.8°C and ΔT_{source} = +1.4°C from LGM to EH. Such a variation of T_{site} over the deglaciation is in fair agreement with the results of *Jouzel et al.* [2003] and the ΔT_{source} is realistic compared to the available estimates of LGM oceanic temperature [*Barrows and Juggins*, 2005; *Sarnthein et al.*, 2003; *Waelbroeck et al.*, 2009]. Surprisingly, we find similar values as in work by *Vimeux et al.* [2002] despite different tunings of the MCIM, because the stronger dependency of d excess to T_{site} in our model is counterbalanced by the strong effect of rh_s.

[57] Taking into account the change in rh_s has a strong influence on the reconstruction of T_{source} (Table 3): for

Table 3. Variations of Site and Source Temperatures Deduced From the Inversion of δ^{18}O and d Excess Changes at Vostok Over the Last Deglaciation, Assuming Different rh_s Variations[a]

Δrh_s (%)	ΔT_{site} (°C)	ΔT_{source} (°C)
−20	+7.8	+1.3
−10	+8.5	+4.4
0	+9.2	+7.4

[a]Δ refers to Early Holocene minus Last Glacial Maximum. T_{site}, site temperature; T_{source}, source temperature.

example, assuming a constant rh_s from LGM to EH yields T_{site} and T_{source} changes of +7.4°C and +9.2°C, respectively. The reconstruction of ΔT_{source} is twice more sensitive to the assumed Δrh_s than ΔT_{site}. Estimating the past rh_s variations through ^{17}O excess measurements would thus have a strong impact on past temperature reconstructions, strengthening the added value of ^{17}O excess measurements.

[58] This calculation contains many uncertainties: tuning of the MCIM, linearity assumption, uncertainties related to the SCM, uncertainties in the exact change of rh_s if part of the change should be attributed to convective changes, to the evaporative recharge, to the seasonal cycle or to other processes not considered here.

[59] To estimate the uncertainties related to the linearity assumption and the neglect of convection in our simplified equations (e.g., equations (4) and (5)), we performed experiments using rh_s, T_{source} and T_{site} variations given in Table 3. To do so, for each Δrh_s scenario, we perform simulations of the isotopic composition of the Vostok ice for the LGM and EH by the SCM and MCIM (Table 4). The inputs of the SCM and MCIM are such that the change of rh_s, T_{source} and T_{site} between EH and LGM (columns 9, 10 and 12 of Table 4) are almost identical to those in Table 3. Changes in rh_s are obtained in the SCM either by varying V_s or ω (column 3 of Table 4), or both simultaneously when ω variations only are not sufficient to explain rh_s variations. We take EH conditions from the control simulation (except when the change in rh_s was impossible to simulate through reasonable V_s or ω variations), but we focus on the EH-LGM differences rather than on the absolute values. Simulations show that whatever the method to vary rh_s in the SCM, be it through an extreme variation of V_s or of convective activity, the simulated EH-LGM change in ^{17}O excess (in per meg) corresponds to the change in rh_s (in %), with an error of 2 per meg maximum (last column of Table 4). Taking a slope of 1 per meg/% and neglecting the effect of convective processes on ^{17}O excess are thus very robust assumptions. Simulated changes in δ^{18}O and d excess in ice are similar to observations with maximum errors of 1.5 and 1.1‰, respectively (columns 16 and 17 of Table 4). This translates into uncertainties of 2.2 and 2.4°C on the reconstruction of ΔT_{site} and ΔT_{source}, respectively.

[60] To estimate the uncertainties related to the models, we perform sensitivity tests with the SCM and the MCIM. We vary tunable parameters in the SCM (auxiliary material Text S1, section 2) and in the MCIM (within ranges of values for which the modeled evolutions of ^{17}O excess and d excess in Antarctica still agree with the data). In the highest deviation from the inversion presented above, obtained by an extreme tuning of the SCM, the reconstruction of T_{site} is virtually unchanged (−0.2°C) whereas the reconstruction of T_{source} is more affected (−1.9°C).

[61] Therefore, when considering the uncertainties mentioned above, the maximum uncertainty ranges for T_{site} and T_{source} are on the order of 2°C and 4°C, respectively. However, the major source of uncertainty in this reconstruction remains the estimated change in rh_s, if other factors than rh_s contribute to the observed ^{17}O excess shift (Table 3): 0.4°C for ΔT_{site} and 9°C for ΔT_{source}.

6. Conclusion

6.1. Summary

[62] We have explored various processes, both at the evaporative source and during the poleward transport, that could explain the +20 per meg increase over the last deglaciation.

[63] Using a single-column model (SCM) over tropical and subtropical oceans, we show that the ^{17}O excess of the low-level vapor is affected mainly by the relative humidity at the surface, rh_s, with a sensitivity of −1.0 per meg/%. This sensitivity is robust and similar to that predicted by the closure assumption, so that it can likely be extended to all latitudes. Given this sensitivity, a 12 to 22% increase in rh_s would be necessary to explain the +20 per meg increase over the last deglaciation. Changes in rain rates over tropical or subtropical sources, conversely, are not likely to contribute to more than a few per meg to the shift.

[64] Using a Rayleigh type distillation model, we show that the amplitude of ^{17}O excess variations in the moisture source regions is well recorded in the ^{17}O excess of the polar precipitation, while they are damped in d excess. The ^{17}O excess in polar snowfall can also be influenced by evaporative recharge and by the amplitude of the δ^{18}O seasonal cycle at the precipitation site, but the contribution of these effects to the observed ^{17}O excess shift is expected to remain secondary (at most 35% of the shift).

[65] Among the different processes considered in this study (changes in convective activity, SST or relative humidity at source regions, in evaporative discharge over midlatitude to high-latitude oceans, in the seasonal cycle of Antarctica precipitation), only one can explain the large magnitude (+20 per meg) of the ^{17}O excess shift observed in Antarctica over the deglaciation: the decrease of the surface relative humidity (rh_s) by 8–22% from LGM to present (in agreement with *Landais et al.* [2008]). This might arise either through a decrease of the surface air relative humidity (rh_a), or through an increase of the thermodynamical disequilibrium between the surface and the near-surface air as the global mean temperature increases.

[66] The fact that current GCMs do not simulate any large change in rh_s during the LGM raises questions. This mismatch could have a link with the inability of current isotopic GCMs to simulate the observed increase of d excess from LGM to EH over polar regions [*Werner et al.*, 2001]: if GCMs simulated a higher rh_s during the LGM, they would more likely simulate a lower d excess, closer to observations.

[67] The possibility of such a large change in rh_s strengthens the interest of ^{17}O excess to provide more accurate reconstructions of source and site temperatures than from the combination of δ^{18}O and d excess only. The assumption

Table 4. Simulations to Estimate the Uncertainties Related to the Linearity Assumption and the Neglect of Convection When Inferring T_{site}, T_{source}, and rh_s From $\delta^{18}O$, d Excess, and ^{17}O Excess in the Vostok Ice[a]

Simulation	Δrh_s Scenario	Method	Age	T_{so} (°C)	V_s (m/s)	ω (hPa/d)	rh_s (%)	Δrh_s (%)	ΔT_{so} (°C)	T_{si} (°C)	ΔT_{si} (°C)	$\delta^{18}O_i$ (‰)	d_i (‰)	$^{17}O_i$ (per meg)	$\Delta\delta^{18}{}_i$ (‰)	Δd_i (‰)	$\Delta^{17}O_i$ (per meg)
1	−20	V_s	EH	29	2	0	56.0			−55		−55.96	23.1	57			
2	−20	V_s	LGM	27.7	6.9	0	76.3	−20.3	1.3	−62.8	7.8	−61.57	23.2	37	5.61	−0.1	20
3	−20	ω and V_s	EH	29	4.5	−90	61.2			−55		−56.01	22.9	52			
4	−20	ω and V_s	LGM	27.7	6.5	30	80.5	−19.3	1.3	−62.8	7.8	−61.85	21.2	32	5.84	1.7	20
5	−10	V_s	EH	29	3.6	15	65.6			−55		−55.64	18.0	47			
6	−10	V_s	LGM	24.6	6.9	15	75.9	−10.3	4.4	−63.5	8.5	−61.60	16.3	37	5.96	1.7	10
7	−10	ω	EH	29	5	−45	66.2			−55		−54.88	21.0	47			
8	−10	ω	LGM	24.6	5	30	76.5	−10.3	4.4	−63.5	8.5	−61.48	19.2	37	6.60	1.8	10
Control	0	V_s	EH	29	5	15	72.5			−55		−54.2	15	42			
9	0	V_s	LGM	21.6	4.5	15	72.3	0.2	7.4	−64.2	9.2	−61.86	14.3	40	7.66	0.7	2
Control	0	ω	EH	29	5	15	72.5			−55		−54.2	15	42			
10	0	ω	LGM	21.6	5	13	72.1	0.4	7.4	−64.2	9.2	−62.15	14.2	40	7.95	0.8	2

[a]We simulate the Vostok ice composition for both the EH and the LGM (Age) corresponding to the scenarios of change in rh_s (Δrh_s Scenario), in sea surface temperature of the source (ΔT_{so}), and in the polar temperature (ΔT_{si}). For each scenario, we vary rh_s in the SCM by two methods (Method): wind speed (V_s) or large-scale vertical velocity at 500 hPa (ω), or both simultaneously when ω variations alone are not sufficient to explain Δrh_s (simulations 3 and 4). For each scenario and method of rh_s variation, we perform two simulations, one for EH and one for LGM (Age column), so that the Δrh_s is as close as possible to the Δrh_s scenario. The inputs of the SCM (sea surface temperature T_{so}, V_s, and ω) used to achieve the Δrh_s scenario are given in columns 5, 6, and 7. The rh_s simulated by the SCM as well as the Δrh_s between EH and LGM are listed in columns 8 and 9. The outputs of the SCM are then used as input for the MCIM, together with the polar temperature (T_{si}). The Vostok ice composition ($\delta^{18}O$, d excess, and ^{17}O excess) simulated by the MCIM is given in columns 13, 14, and 15, and the corresponding EH-LGM variations for each scenario and method of rh_s variation are given in columns 16, 17, and 18. These simulated variations are to be compared with the observed +7‰, +1‰, and +20 per meg for Vostok ice $\delta^{18}O$, d excess, and ^{17}O excess, respectively. Note that we focus here on the EH-LGM differences, rather than on the absolute values.

that rh_s changes are either negligible or linearly related to temperature [*Vimeux et al.*, 2001; *Stenni et al.*, 2001] can be relaxed. Using ^{17}O excess measurements to constrain the change in rh_s yields a LGM source temperature about 1.4°C lower than at EH, and a Vostok temperature 7.8°C lower. Both these estimates are consistent with previous studies [*Vimeux et al.*, 2001], but owing to compensating effects. These estimates are particularly sensitive to the reconstructed change in rh_s.

6.2. Perspectives

[68] While we explore the influence of different climate conditions both at the evaporative source and during the poleward transport, our approach is still incomplete. First, we considered only one evaporative source and one trajectory, whereas the polar snowfall originates from different sources through various trajectories [e.g., *Helsen et al.*, 2006]. Given the sensitivity of ^{17}O excess of mixing of contrasted $\delta^{18}O$ moisture, the heterogeneity of the sources could have an impact on the polar ^{17}O excess. Second, the SCM was run for subtropical conditions, whereas middle and high latitudes are also important sources of vapor for Antarctica snowfall [*Delaygue et al.*, 2000; *Werner et al.*, 2001]. Whereas the sensitivity of the isotopic composition of low-level vapor to surface relative humidity can be applied to all latitudes [*Jouzel et al.*, 1982; *Landais et al.*, 2008], the sensitivity to tropical convective processes is more difficult to generalize to extratropical latitudes. In addition, some effects controlling the ice ^{17}O excess in middle and high latitudes might have been ignored. For example, 3D large-scale advections or changes in cloud dynamics and microphysics in frontal systems [*Gedzelman and Arnold*, 1994] might play an important role. The type of water transport (diffusive or advective [*Hendricks et al.*, 2000; *Kavanaugh and Cuffey*, 2003] might also affect the ^{17}O excess, since diffusive transport would involve some mixing, which decreases the ^{17}O excess due to the nonlinearity of the mixing curves in the logarithmic diagram (Figure 2). GCM simulations with isotopic capabilities including $H_2^{17}O$ would be necessary to explore these processes and thus to better understand what information is recorded in snowfall ^{17}O excess.

Appendix A: Description of the Single-Column Model

A1. Physical Package

[69] The SCM includes bulk formulas for sea surface evaporation, a radiation parametrization [*Fouquart and Bonnel*, 1980; *Morcrette*, 1991], the Emanuel convective parametrization [*Emanuel*, 1991; *Emanuel and Zivkovic-Rothman*, 1999] and a statistical cloud scheme coupled to this convective scheme [*Bony and Emanuel*, 2001]. The only dimension is altitude, discretized with 40 pressure levels. A complete description of the isotopic and nonisotopic aspects of this model is given by *Bony et al.* [2008] and *Bony and Emanuel* [2001], respectively.

[70] The convective parametrization represents the net effect on the large-scale environment of an ensemble of convective systems. Air parcels from the BL are adiabatically lifted to different levels until they precipitate. The falling precipitation partially or totally reevaporates as it falls through unsaturated atmospheric layers, driving an unsaturated downdraft.

[71] The boundary conditions of this model are surface conditions (surface wind, sea surface temperature and albedo), insolation, CO_2 and large-scale atmospheric forcing. Large-scale vertical motions control the convective activity: for example, a large-scale ascent is associated with large-scale moisture convergence and thus strong convection. In the model, the large-scale circulation is represented by a large-scale ascent or descent, prescribed as a vertical profile of vertical velocity of cubic shape.

[72] Horizontal advections of temperature and humidity are computed from the large-scale velocity. Horizontal gradients of temperature and humidity are neglected, as justified by *Bony et al.* [2008] over tropical oceans.

A2. Representation of Isotopic Processes

[73] The representation of isotopic processes is described in detail by *Bony et al.* [2008]. Water isotopic species ($H_2^{16}O$, $H_2^{17}O$, $H_2^{18}O$ and HDO) are passively transported by the large-scale and convective mass fluxes. As for humidity, horizontal isotopic gradients are neglected. Isotopic fractionation is introduced at each phase change, with fractionation coefficients for $H_2^{18}O$ and HDO given by *Bony et al.* [2008]. For $H_2^{17}O$, we took the experimental values determined by *Barkan and Luz* [2005, 2007] for liquid-vapor equilibrium fractionation and kinetic fractionation. For solid-vapor equilibrium fractionation coefficients, in the absence of experimental determination, we took the theoretical determination by *Van Hook* [1968].

[74] Isotopic fractionation during surface evaporation is represented by the *Craig and Gordon* [1965] equation (equation (1) of the auxiliary material Text S1). The kinetic fractionation coefficient α_K depends on surface wind speed V_s according to *Merlivat and Jouzel* [1979]. For V_s below 7 m/s, which represents 95% of the ocean surface [*Eriksson and Bolin*, 1964], the kinetic fractionation coefficient is constant.

[75] We assume isotopic equilibrium with the vapor for liquid condensation (above 0°C), and a Rayleigh distillation for ice condensation (below −15°C). Between 0°C and −15°C, the composition of the condensate is assumed to be a linear combination of the compositions of the liquid and solid phases.

[76] Following *Jouzel and Merlivat* [1984], we take into account kinetic effects due to supersaturation with respect to ice S_i, assuming that S_i varies linearly as a function of temperature T,

$$S_i = \mu - \lambda \cdot T \tag{A1}$$

where μ and λ are tunable parameters [*Jouzel and Merlivat*, 1984]; μ is set to 1 [e.g., *Hoffmann et al.*, 1998; *Noone and Simmonds*, 2002]. λ has typical values of 0.002 [e.g., *Landais et al.*, 2008], 0.003 [e.g., *Hoffmann et al.*, 1998; *Noone and Simmonds*, 2002] or 0.004 [e.g., *Schmidt et al.*, 2007; *Vimeux et al.*, 2001; *Stenni et al.*, 2001]. Here we take $\lambda = 0.002$ to be consistent with *Landais et al.* [2008], who used both d excess and ^{17}O excess data to constrain λ.

[77] In the unsaturated downdraft, sublimation of ice is assumed not to fractionate due to low isotopic diffusivities in ice.

[78] Fractionation during rain reevaporation and diffusive exchanges between rain and vapor are represented following Stewart's model [*Stewart*, 1975], as described by *Bony et al.* [2008]. In this model, the evolution of the isotopic composition of the rain drops is calculated using mass conservation equations and assuming that at each instant, the isotopic composition of the rain evaporation R_e is given by *Craig and Gordon* [1965]:

$$R_e = \left(\frac{D'}{D}\right)^n \cdot \frac{\frac{R_l}{\alpha_{eq}} - h_{eff} \cdot R_b}{1 - h_{eff}} \tag{A2}$$

where R_l is the isotopic composition of the rain, R_b the isotopic composition of the vapor in the unsaturated downdraft (i.e., surrounding the rain shaft) and h_{eff} is the relative humidity at the droplets surface. D and D' are the diffusivities of water and isotopic species, respectively, taken from *Merlivat* [1978], and n is an exponent set to 0.58 [*Stewart*, 1975]. The h_{eff} is parameterized as a function of the relative humidity in the unsaturated downdraft h_{dd} as

$$h_{eff} = \phi + (1 - \phi) \cdot h_{dd}, \tag{A3}$$

with ϕ a tunable parameter between 0 and 1. This parameter represents the humidification around the rain drops and controls how much the rain drops reequilibrate with the unsaturated downdraft vapor by diffusive exchange: if $h_{eff} = 0$, no diffusion occurs. If $h_{eff} = 1$, only diffusive exchanges occur and the vapor and the droplets tend toward isotopic equilibrium. The ϕ is set to 0.9 to optimize the simulation of the isotopic composition of the tropical rain [*Bony et al.*, 2008]. The isotopic composition of the rain R_l and the downdraft vapor R_b are then calculated using mass balance equations for both water and isotopic species.

Appendix B: Distillation Model MCIM

[79] To model the evolution of the isotopic composition of air masses from the source region to the poles as well as the composition of the Vostok snowfall, we use the Mixed Cloud Isotopic Model (MCIM) [*Ciais and Jouzel*, 1994] adapted for the calculation of ice ^{17}O excess [*Landais et al.*, 2008], with the same fractionation coefficients as in the SCM.

[80] The MCIM is an extension of Lagrangian models based on a Rayleigh distillation [*Merlivat and Jouzel*, 1979; *Jouzel and Merlivat*, 1984]. It describes the isotopic processes at each phase transition and thus the isotopic composition of (1) the condensed phase (liquid water or solid ice) and (2) the water vapor at each step from the oceanic source region to the precipitation site on the ice sheet. During liquid precipitation, only equilibrium fractionation occurs. Then, kinetic fractionation is taken into account for snowflakes formation. Depending on the temperature, the MCIM allows for a zone of mixed clouds, where liquid droplets and ice crystal can coexist. In this zone, the Bergeron-Findeisen process associated with significant kinetic fractionation effects is considered (details given by *Ciais and Jouzel* [1994]). As for the SCM, the relative proportion of equilibrium versus kinetic fractionation is controlled by the supersaturation.

[81] The transport path of the water mass is described in terms of temperature and pressure. The air parcel is transported in saturated (or supersaturated in polar regions) conditions from the source region to the precipitation site, hence implying continuous fractionation. In nature, air parcels are transported

mainly in unsaturated conditions and most of the saturation occurs during the last day of transport [*Helsen et al.*, 2006]. However, since the depletion associated with the distillation depends mainly on the initial and final temperatures, considering transport in saturated conditions has little impact on the results (less than 2‰ for δ^{18}O, and negligible for d excess [*Helsen et al.*, 2006]).

[82] The model receives as main inputs (1) the temperature and pressure of the source region as well as the isotopic composition of the initial water vapor and (2) the temperature and pressure at the precipitation site.

[83] The MCIM includes several tunable parameters [*Ciais and Jouzel*, 1994] such as the dependence of supersaturation on temperature, the fraction of condensate remaining in clouds. We performed numerous sensitivity experiments to tune these parameters and kept only those enabling a reproduction of the δ^{18}O, d excess and ^{17}O excess on the Antarctic transect [*Landais et al.*, 2008]. Note that the same dependency of supersaturation with temperature has been taken for the MCIM and the SCM. For the other tunable parameters, we choose values very similar to those used in previous studies [*Ciais and Jouzel*, 1994; *Vimeux et al.*, 2001; *Stenni et al.*, 2001]. Other parameters have however been tested (section 5).

[84] **Acknowledgments.** The first two authors contributed equally to this work. We thank Masa Kageyama for useful discussions. This work benefited from financial support of the French Agence Nationale for Research, and from the LEFE project MISSTERRE. We acknowledge the international modeling groups for providing the PMIP2 data for analysis and the Laboratoire des Sciences du Climat et de l'Environnement (LSCE) for collecting and archiving the model data. The PMIP2/MOTIF Data Archive is supported by CEA, CNRS, the EU project MOTIF (EVK2-CT-2002-00153), and the Programme National d'Etude de la Dynamique du Climat (PNEDC). The analyses were performed using the version available in October 2008. More information is available at http://pmip2.lsce.ipsl.fr/ and http://motif.lsce.ipsl.fr/. We thank two anonymous reviewers for their comments and suggestions.

References

Angert, A., J.-E. Lee, and D. Yakir (2008), Seasonal variations in the isotopic composition of near-surface water vapour in the eastern Mediterranean, *Tellus, Ser. B*, *60*, 674–684.

Barkan, E., and B. Luz (2005), High precision measurements of $^{17}O/^{16}O$ and $^{18}O/^{16}O$ ratios in H_2O, *Rapid Commun. Mass Spectrom.*, *19*, 3737–3742.

Barkan, E., and B. Luz (2007), Diffusivity fractionations of $H_2^{16}O/H_2^{17}O$ and $H_2^{16}O/H_2^{18}O$ in air and their implications for isotope hydrology, *Rapid Commun. Mass Spectrom.*, *21*, 2999–3005.

Barrows, T., and S. Juggins (2005), Sea-surface temperatures around the Australian margin and Indian Ocean during the Last Glacial Maximum, *Quat. Sci. Rev.*, *24*, 1017–1047.

Bony, S., and K. A. Emanuel (2001), A parameterization of the cloudiness associated with cumulus convection: Evaluation using TOGA COARE data, *J. Atmos. Sci.*, *58*, 3158–3183.

Bony, S., J.-L. Dufresne, H. Le Treut, J.-J. Morcrette, and C. Senior (2004), On dynamic and thermodynamic components of cloud changes, *Clim. Dyn.*, *22*, 71–86, doi:10.1007/s00382-003-0369-6.

Bony, S., et al. (2006), How well do we understand and evaluate climate change feedback processes?, *J. Clim.*, *19*, 3445–3482.

Bony, S., C. Risi, and F. Vimeux (2008), Influence of convective processes on the isotopic composition (δ^{18}O and δD) of precipitation and water vapor in the tropics: 1. Radiative-convective equilibrium and Tropical Ocean-Global Atmosphere-Coupled Ocean-Atmosphere Response Experiment (TOGA-COARE) simulations, *J. Geophys. Res.*, *113*, D19305, doi:10.1029/2008JD009942.

Braconnot, P., et al. (2007), Results of PMIP2 coupled simulations of the Mid-Holocene and Last Glacial Maximum—Part 1: Experiments and large-scale features, *Clim. Past*, *3*, 261–277.

Bush, A. B., and S. G. H. Philander (1999), The climate of the Last Glacial Maximum: Results from a coupled atmosphere-ocean general circulation model, *J. Geophys. Res.*, *104*, 24,509–24,525.

Chiang, J. C. H., and C. M. Bitz (2005), Influence of high latitude ice cover on the marine Intertropical Convergence Zone, *Clim. Dyn.*, *25*, 477–496.

Ciais, P., and J. Jouzel (1994), Deuterium and oxygen 18 in precipitation: Isotopic model, including cloud processes, *J. Geophys. Res.*, *99*, 16,793–16,803.

Ciais, P., W. White, J. Jouzel, and J. Petit (1995), The origin of present-day Antarctic precipitation from surface snow deuterium excess data, *J. Geophys. Res.*, *100*, 18,917–18,927, doi:10.1029/95JD01169.

Craig, H. (1961), Isotopic variations in meteoric waters, *Science*, *133*, 1702–1703.

Craig, H., and L. I. Gordon (1965), Deuterium and oxygen-18 variations in the ocean and marine atmosphere, in *Proceedings of a Conference on Stable Isotopes in Oceanographic Studies and Paleotemperatures*, edited by E. Tongiorgi, pp. 9–130, Lischi and Figli, Pisa, Italy.

Cuffey, K., and F. Vimeux (2001), Covariation of carbon dioxide and temperature from the Vostok ice core after deuterium-excess correction, *Nature*, *412*, 523–527.

Dahe, Q., J. R. Petit, J. Jouzel, and M. Stievenard (1994), Distribution of stable isotopes in surface snow along the route of the 1990 International Trans-Antarctica Expedition, *J. Glaciol.*, *40*, 107–118.

Dansgaard, W. (1953), The abundance of ^{18}O in atmospheric water and water vapour, *Tellus*, *5*, 461–469.

Dansgaard, W. (1964), Stable isotope in precipitation, *Tellus*, *16*, 436–468.

Delaygue, G. (2000), Relations entre surface ocanique et composition isotopique des prcipitations antarctiques: simulations pour diffrents climats, Ph.D. thesis, Univ. d'Aix-Marseille III, Marseille, France.

Delaygue, G., V. Masson, J. Jouzel, R. D. Koster, and R. J. Healy (2000), The origin of Antarctic precipitation: A modelling approach, *Tellus, Ser. B*, *52*, 19–36.

Delmotte, M., V. Masson, J. Jouzel, and V. Morgan (2000), A seasonal deuterium excess signal at Law Dome, coastal eastern Antarctica: A Southern Ocean signature, *J. Geophys. Res.*, *105*, 7187–7197, doi:10.1029/1999JD901085.

Ekaykin, A. (2003), Meteorological regime of central Antarctic and its role in the formation of isotope composition of snow thickness, Ph.D. thesis, Univ. Grenoble 1-Joseph Fourier, Grenoble, France.

Ekaykin, A. A., and V. Y. Lipenkov (2008), Formation of the ice core isotope composition, paper presented at 2nd International Workshop on Physics of Ice Core Records (PICR-2), Hokkaido Univ., Sapporo, Japan.

Emanuel, K. A. (1991), A scheme for representing cumulus convection in large-scale models, *J. Atmos. Sci.*, *48*, 2313–2329.

Emanuel, K. A., and M. Zivkovic-Rothman (1999), Development and evaluation of a convection scheme for use in climate models, *J. Atmos. Sci.*, *56*, 1766–1782.

Epstein, S., and T. Mayeda (1953), Variations of O18 content of waters from natural sources, *Geochim. Cosmochim. Acta*, *4*, 213–224.

Eriksson, E., and B. Bolin (1964), Oxygen-18, deuterium and tritium in natural waters and their relations to the global circulation of water, paper presented at Second Conference on Radioactive Fallout From Nuclear Weapon Tests, U.S. At. Energy Comm., Germantown, Md.

Fouquart, Y., and B. Bonnel (1980), Computation of solar heating of the Earth's atmosphere: A new parameterization, *Beitr. Phys. Atmos.*, *53*, 35–62.

Gat, J. R. (1996), Oxygen and hydrogen isotopes in the hydrologic cycle, *Ann. Rev. Earth Planet. Sci.*, *24*, 225–262.

Gedzelman, S. D., and R. Arnold (1994), Modeling the isotopic composition of precipitation, *J. Geophys. Res.*, *99*, 10,455–10,472, doi:10.1029/93JD03518.

Harrison, S. (2000), Palaeoenvironmental data sets and model evaluation in PMIP, in *Paleoclimate Modelling Intercomparison Project (PMIP)*, edited by P. Braconnot, *WMO/TD-1007*, pp. 9–25, World Meteorol. Org., Geneva, Switzerland.

Helsen, M. M., R. S. W. van de Wal, V. van den Broeke, M. R. Masson-Delmotte, H. A. J. Meijer, M. P. Scheele, and M. Werner (2006), Modeling the isotopic composition of Antarctic snow using backward trajectories: Simulation of snow pit records, *J. Geophys. Res.*, *111*, D15109, doi:10.1029/2005JD006524.

Hendricks, M., D. DePaolo, and R. Cohen (2000), Space and time variation of δ^{18}O and δD in precipitation: Can paelotemperatures be estimated from ice cores?, *Global Biogeochem. Cycles*, *14*, 851–861, doi:10.1029/1999GB001198.

Hoffmann, G., M. Werner, and M. Heimann (1998), Water isotope module of the ECHAM atmospheric general circulation model: A study on timescales from days to several years, *J. Geophys. Res.*, *103*, 16,871–16,896, doi:10.1029/98JD00423.

Johnsen, S., W. Dansgaard, and J. White (1989), Origin of arctic precipitation under present and glacial conditions, *Tellus, Ser. B*, *41*, 452–458.

Jouzel, J. (2003), Water stable isotopes: Atmospheric composition and applications in polar ice core studies, *Treatise Geochem.*, *4*, 213–243, doi:10.1016/B0-08-043751-6/04040-8.

Jouzel, J., and R. D. Koster (1996), A reconsideration of the initial conditions used for stable water isotope models, *J. Geophys. Res.*, *101*, 22,933–22,938, doi:10.1029/96JD02362.

Jouzel, J., and L. Merlivat (1984), Deuterium and oxygen 18 in precipitation: Modeling of the isotopic effects during snow formation, *J. Geophys. Res.*, *89*, 11,749–11,757, doi:10.1029/JD089iD07p11749.

Jouzel, J., L. Merlivat, and C. Lorius (1982), Deuterium excess in an East Antarctic ice core suggests higher relative humidity at the oceanic surface during the Last Glacial Maximum, *Nature*, *299*, 688–691.

Jouzel, J., R. Koster, R. Suozzo, and G. Russel (1994), Stable water isotope behavior during the Last Glacial Maximum: A general circulation model analysis, *J. Geophys. Res.*, *99*, 25,791–25,801, doi:10.1029/94JD01819.

Jouzel, J., F. Vimeux, N. Caillon, G. Delaygue, G. Hoffmann, V. Masson-Delmotte, and F. Parrenin (2003), Magnitude of isotope/temperature scaling for interpretation of central Antarctic ice cores, *J. Geophys. Res.*, *108*(D12), 4361, doi:10.1029/2002JD002677.

Jouzel, J., M. Stivenard, S. Johnsen, A. Landais, V. Masson-Delmotte, A. Sveinbjornsdottir, F. Vimeux, U. von Grafenstein, and J. White (2007a), The GRIP deuterium-excess record, *Quat. Sci. Rev.*, *26*, 1–17.

Jouzel, J., et al. (2007b), Orbital and millennial Antarctic climate variability over the past 800,000 years, *Science*, *317*, 5839, doi:10.1126/science.1141038.

Kalnay, E., et al. (1996), The NCEP/NCAR 40-year reanalysis project, *Bull. Am. Meteorol. Soc.*, *77*, 437–470.

Kang, S., I. Held, D. Frierson, and M. Zhao (2008), The response of the ITCZ to extratropical thermal forcings: Idealized slab ocean experiments with a GCM, *J. Clim.*, *21*, 3521–3532.

Kavanaugh, J. L., and K. M. Cuffey (2003), Space and time variation of δ^{1}8O and δD in Antarctic precipitation revisited, *Global Biogeochem. Cycles*, *17*(1), 1017, doi:10.1029/2002GB001910.

Laîne, A., M. Kageyama, D. Salas-Mélia, A. Voldoire, G. Riviére, G. Ramstein, S. Planton, S. Tyteca, and J.-Y. Peterschmitt (2008), Northern Hemisphere storm tracks during the Last Glacial Maximum in the PMIP2 ocean-atmosphere coupled models: Energetic study, seasonal cycle, precipitation, *Clim. Dyn.*, *32*, 593–614.

Landais, A., E. Barkan, and B. Luz (2008), Record of δ^{18}O and ^{17}O-excess in ice from Vostok Antarctica during the last 150,000 years, *Geophys. Res. Lett.*, *35*, L02709, doi:10.1029/2007GL032096.

Lawrence, J. R., S. D. Gedzelman, D. Dexheimer, H.-K. Cho, G. D. Carrie, R. Gasparini, C. R. Anderson, K. P. Bowman, and M. I. Biggerstaff (2004), Stable isotopic composition of water vapor in the tropics, *J. Geophys. Res.*, *109*, D06115, doi:10.1029/2003JD004046.

Lee, J.-E., I. Fung, D. DePaolo, and C. C. Fennig (2007), Analysis of the global distribution of water isotopes using the NCAR atmospheric general circulation model, *J. Geophys. Res.*, *112*, D16306, doi:10.1029/2006JD007657.

Lee, J.-E., I. Fung, D. J. DePaolo, and B. Otto-Bliesner (2008), Water isotopes during the Last Glacial Maximum: New general circulation model calculations, *J. Geophys. Res.*, *113*, D19109, doi:10.1029/2008JD009859.

Luz, B., and E. Barkan (2005), The isotopic ratios $^{17}O/^{16}O$ and $^{18}O/^{16}O$ in molecular oxygen and their significance in biogeochemistry, *Geochem. Cosmochim. Acta.*, *69*, 1099–1110.

Masson-Delmotte, V., et al. (2005), Holocene climatic changes in Greenland: Different deuterium excess signals at Greenland Ice Core Project (GRIP) and NorthGRIP, *J. Geophys. Res.*, *110*, D14102, doi:10.1029/2004JD005575.

Masson-Delmotte, V., et al. (2008), A review of Antarctic surface snow isotopic composition: Observations, atmospheric circulation and isotopic modelling, *J. Clim.*, *21*, 3359–3387.

Merlivat, L. (1978), Molecular diffusivities of $H_2^{16}O$, $HD^{16}O$, and $H_2^{18}O$ in gases, *J. Chem. Phys.*, *69*, 2864–2871.

Merlivat, L., and J. Jouzel (1979), Global climatic interpretation of the ddeuterium-oxygen 18 relationship for precipitation, *J. Geophys. Res.*, *84*, 5029–5332, doi:10.1029/JC084iC08p05029.

Merlivat, L., and G. Nief (1967), Fractionnement isotopique lors des changements d'états solide-vapeur et liquide-vapeur de l'eau à des températures inférieures à °C, *Tellus*, *19*, 122–127.

Morcrette, J.-J. (1991), Radiation and cloud radiative properties in the European Centre for Medium-range Weather Forecasts forecasting system, *J. Geophys. Res.*, *96*, 9121–9132, doi:10.1029/89JD01597.

Noone, D. (2008), The influence of midlatitude and tropical overturning circulation on the isotopic composition of atmospheric water vapor and Antarctic precipitation, *J. Geophys. Res.*, *113*, D04102, doi:10.1029/2007JD008892.

Noone, D., and I. Simmonds (2002), Associations between δ^{18}O of water and climate parameters in a simulation of atmospheric circulation for 1979–95, *J. Clim.*, *15*, 3150–3169.

Petit, J., M. Briat, and A. Royer (1981), Ice age aerosol content from east Antarctic ice cores samples and past wind strength, *Nature*, *293*, 391–394.

Petit, J. R., J. W. C. White, N. W. Young, J. Jouzel, and Y. S. Korotkevich (1991), Deuterium excess in recent Antarctic snow, *J. Geophys. Res.*, *96*, 5113–5122.

Petit, J. R., et al. (1999), 420,000 years of climate and atmopheric history revealed by the Vostok deep Antarctic ice core, *Nature*, *399*, 429–436.

Pfahl, S., and H. Wernli (2008), Air parcel trajectory analysis of stable isotopes in water vapor in the eastern Mediterranean, *J. Geophys. Res.*, *113*, D20104, doi:10.1029/2008JD009839.

Raymond, D. (1995), Regulation of moist convection over the west Pacific warm pool, *J. Atmos. Sci.*, *52*, 3945–3959.

Risi, C., S. Bony, and F. Vimeux (2008), Influence of convective processes on the isotopic composition (δ^{18}O and δD) of precipitation and water vapor in the tropics: 2. Physical interpretation of the amount effect, *J. Geophys. Res.*, *113*, D19306, doi:10.1029/2008JD009943.

Rozanski, K., L. Araguas-Araguas, and R. Gonfiantini (1993), Isotopic patterns in modern global precipitation, in *Climate Change in Continental Isotopic Records*, *Geophys. Monogr. Ser.*, vol. 78, edited by P. K. Swart et al., pp. 1–36, AGU, Washington, D. C.

Sarnthein, M., R. Gersonde, S. Niebler, U. Pflaumann, R. Spielhagen, J. Thiede, G. Wefer, and M. Weinelt (2003), Overview of Glacial Atlantic Ocean Mapping (GLAMAP 2000), *Paleoceanography*, *18*(2), 1030, doi:10.1029/2002PA000769.

Schmidt, G., A. LeGrande, and G. Hoffmann (2007), Water isotope expressions of intrinsic and forced variability in a coupled ocean-atmosphere model, *J. Geophys. Res.*, *112*, D10103, doi:10.1029/2006JD007781.

Sobel, A. H., and C. S. Bretherton (2000), Modeling tropical precipitation in a single column, *J. Clim.*, *13*, 4378–4392.

Stenni, B., V. Masson-Delmotte, S. Johnsen, J. Jouzel, A. Longinelli, E. Monnin, R. Rthlisberger, and E. Selmo (2001), An oceanic cold reversal during the last deglaciation, *Science*, *293*, 2074–2077.

Stewart, M. K. (1975), Stable isotope fractionation due to evaporation and isotopic exchange of falling waterdrops: Applications to atmospheric processes and evaporation of lakes, *J. Geophys. Res.*, *80*, 1133–1146, doi:10.1029/JC080i009p01133.

Toggweiler, J. R., J. L. Russell, and S. R. Carson (2006), Midlatitude westerlies, atmospheric CO_2, and climate change during the ice ages, *Paleoceanography*, *21*, PA2005, doi:10.1029/2005PA001154.

Trenberth, K. (1998), Atmospheric moisture recycling: Role of advection and local evaporation, *J. Clim.*, *12*, 1368–1381.

Uemura, R., Y. Matsui, K. Yoshimura, H. Motoyama, and N. Yoshida (2008), Evidence of deuterium-excess in water vapour as an indicator of ocean surface conditions, *J. Geophys. Res.*, *113*, D19114, doi:10.1029/2008JD010209.

Uemura, R., E. Barkan, O. Abe, and B. Luz (2010), Triple isotope composition of oxygen in atmospheric water vapor, *Geophys. Res. Lett.*, *37*, L04402, doi:10.1029/2009GL041960.

Van Hook, A. (1968), Vapor pressures of the isotopic waters and ices, *J. Phys. Chem.*, *72*, 1234–1244.

Vimeux, F. (1999), Variations de l'Excs en Deutrium en Antarctique au cours des 400 00 dernires annes: Implications climatiques, Ph.D. thesis, Univ. Paris VI, Paris.

Vimeux, F., V. Masson, G. Delaygue, J. Jouzel, J. R. Petit, and M. Stievenard (2001), A 420,000 year deuterium excess record from East Antarctica: Information on past changes in the origin of precipitation at Vostok, *J. Geophys. Res.*, *106*, 31,863–31,873, doi:10.1029/2001JD900076.

Vimeux, F., K. Cuffey, and J. Jouzel (2002), New insights into Southern Hemisphere temperature changes from Vostok ice cores using deuterium excess correction, *Earth Planet. Sci. Lett.*, *203*, 829–843.

Waelbroeck, C., et al. (2009), Constraints on the magnitude and patterns of ocean cooling at the Last Glacial Maximum, *Nat. Geosci.*, *2*, 127–132, doi:10.1038/ngeo411.

Werner, M., M. Heimann, and G. Hoffmann (2001), Isotopic composition and origin of polar precipitation in present and glacial climate simulations, *Tellus, Ser. B*, *53*, 53–71, doi:10.1034/j.1600-0889.2001.01154.x.

S. Bony and C. Risi, LMD, IPSL, UPMC, CNRS, 4, Place Jussieu, F-75005 Paris, France. (crlmd@lmd.jussieu.fr)

J. Jouzel, A. Landais, and V. Masson-Delmotte, LSCE, IPSL, CEA, CNRS, UVSQ, Bt. 701, Orme des Merisiers, F-91191 Gif-sur-Yvette, France.

F. Vimeux, UR Great Ice, IRD, LSCE, IPSL, CEA, CNRS, UVSQ, Bt. 701, Orme des Merisiers, F-91191 Gif-sur-Yvette, France.